# Collimated proton beam from an ultra-intense laser pulse irradiating parallel to the plasmas interface

M. Masum Haider* and Zheng-Mao Sheng
*Institute for Fusion Theory and Simulation, Department of Physics, Zhejiang University, Hangzhou 310027, China*

Recently, there has been some works on surface plasma wave (SPW) excited by a laser obliquely irradiating on thin foil target, which can cause stronger target normal sheath acceleration of protons, but cannot be excited by a grazing incidence laser. Here, we demonstrate a large amplitude Interface Plasma Wave (IPW) can be excited by a relativistic laser pulse irradiating parallel (or grazing incidence) to the interface of solid aluminum and low density hydrogen layer. This IPW enhance markedly sheath electric field to accelerate proton and reduce reflection of laser pulse to improve the couple efficiency. As results, a collimated high energetic and lower energy spread proton beam can be efficiently achieved.

## I. INTRODUCTION

In the early 90s of the last century, the introduction of the chirped-pulse-amplification technique to generate high power, short pulse lasers open a new era in ion acceleration from laser-solid interactions. Due to the higher charge-to-mass ratio, protons accelerate preferentially from either side of the targets [1–4]. The unique characteristics (high energy, short pulse duration, high current, low emittance, and good directionality) of the proton beam, emitted from the back of the solid targets, make it suitable for particularly promising applications in several branches of science and technology like nuclear physics, experimental astrophysics, hadron therapy, warm dense matter, inertial confinement fusions and so on. [5–9]. It is noticed that the generation of protons from laser-solid interactions depends not only on the laser parameters like intensity, pulse duration, prepulse level but also target properties like thickness, geometry, material, etc. [2, 4].

One of the foremost acceleration of the rear surface is target normal sheath acceleration (TNSA)[10, 11], and investigated by many groups in the last few decades. However, due to its relatively low experimental requirements compared with other schemes (e.g., radiation pressure acceleration, collisionless shock acceleration), TNSA is the most studied laser-induced proton acceleration mechanism [9, 12]. In this mechanism, an intense ultrashort laser pulse irradiates a solid foil with hydrogen contamination or an absorbing layer on the rear. It quickly converts the foil into an overdense plasma and penetrates the skin layer, where the laser field falls off rapidly with depth. The laser experts a strong pondermotive force on electrons and pushes them forward. The expansion of the energized electrons, into the vacuum, provokes a sheath electric field in the $TVm^{-1}$ range essentially normal to the target surface. Therefore, this sheath field accelerates the protons from hydrogen-containing contaminants on the foil surface up to MeV energies over just a few micrometers.

Recent studies show that structured targets can enhance the level of laser absorption [13, 14], and the radiation yield [14, 15]. On the other hand, the physical parameters of electron and ion beams can be improved via excitation of surface plasmons, i.e., surface plasma waves [16]. Seshardi, Toda, Hirota, and Suzuki have performed pioneering studies of surface plasma waves that were propagated transversely to an external magnetic field [17–21]. The surface plasma waves or simply, the surface waves (SWs) are localized electron oscillation modes that can be excited at the vacuum-plasma interface by a laser field that irradiates a periodically modulated surface[14]. Using the dielectric constants of the media, $\epsilon_1$ and $\epsilon_2(\omega) = 1-(\omega_p/\omega)^2$, the dispersion relation of the SWs reads as: $k_{SW(\omega)} = \omega/c\sqrt{\epsilon_1\epsilon_2/(\epsilon_1+\epsilon_2)} = \omega/c\sqrt{(1-\eta)/(2-\eta)}$. Here, $\eta = (\omega_p/\omega)^2 = n_e/n_c$ represents the plasma parameter, $\omega_p = \sqrt{n_e e^2/m_e\epsilon}$ is the plasma frequency and $n_c = m_e\epsilon_0\omega_L^2/e^2$ is the plasma critical density, $e$, and $m_e$ is the charge and rest mass of an electron, respectively, $n_e$ is the number density of electrons, $c$ is the speed of light in vacuum, and $\omega_L$ is the laser frequency.

In the presence of a static magnetic field, Chauhan et al. [22] considered the electron acceleration during the resonant interaction of launched electron pulse with surface plasma wave, and consequently, accelerates the electrons at moderate relative intensity by SWs excited with double-metal surface configuration. Varaki [23] had studied the electron acceleration by an SW propagating through two parallel metal sheets. Earlier, electron SWs in a metal bond plasma slab have been detected and analyzed by Cooperbarg [24]. Recently, Zhu et. al. [14] studied the process of high energy electron acceleration onward the surface of the grating targets irradiated by a relativistic, high-contrast laser pulse at an intensity $2.5\times10^{20}\mathrm{Wcm}^{-2}$. The theoretical and experimental studies of electron acceleration by the evanescent field of the SWs, demonstrate that the SWs excitation has a direct impact that leads to improved physical parameters; such as enhanced flux and charge density of the electrons, a higher electron maximum energy, and a higher absorp-

*Permanent address: Department of Physics, Mawlana Bhashani Science and Technology University, Tangail-1902,Bangladesh

tion efficiency [14, 16, 25–28]. Liu et. al. [29] had shown that the amplitude of surface wave depends on the laser incidence angle $\theta_i$. At normal laser incidence, the SW amplitude is smaller than that at $\theta_i = 45°$, and falls off to zero at grazing incidence ($\theta_i = 90°$).

Here we investigate an ultra-intense laser pulse irradiating parallel to the plasmas interface between aluminum and hydrogen thin layer to generate an electron interface wave (IW) which accelerates the protons with higher kinetic energy. Compared to the proton acceleration from the rear side of the solid-target due to the incident laser pulse, normal to the target (Direction-1 in Fig.1), propagating parallel laser pulse towards the target interface (Direction-2 in Fig.1) shows a promising hope in laser-to-plasma conversion efficiency and beam characteristics as well. Our investigation also extends to various laser intensity.

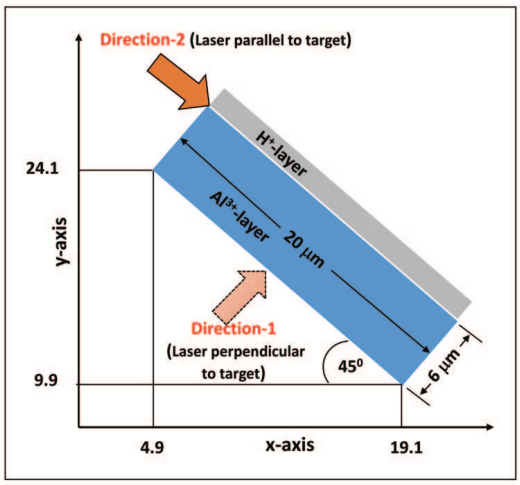


FIG. 1: Schematic diagram of the solid aluminum target of density 2.7 gm/cc attached with a 100nm contaminant hydrogen layer. The target slab is placed in such a manner (making an angle 45° with the $x$-axis) that we may study the effect of the parallel and perpendicular laser pulse to the target without altering its orientation. All over the manuscript, 'Direction-1' indicates the direction of the laser pulse towards the perpendicular to the target at the opposite side of the contaminant H-layer, whereas, 'Direction-2' indicates the laser beam direction towards parallel to the rear interface of the Al target at the junction.

## II. SIMULATION PARAMETER

For numerical analysis, we have used a 2D3V (two-dimensional in space and three-dimensional in velocity Particle-in-cell (PIC) simulation code name OPIC 2.0, which has been verified through particle acceleration through laser-plasma interaction[30–35]. Fig.1 represents the schematic diagram of the target in our simulations. Here, a solid aluminum target inclined at 45° to the $x$-axis. The reason behind the inclination is that it allows us to observe the particle dynamics due to both perpendicular (Direction-1) and parallel (Direction-2) incident laser pulse without altering the target orientation in the simulation box. In this case, the density of the Al target is 2.7 gm/cc, which corresponds to $60n_c$ having ionization 3. The chosen thickness of the aluminum foil varies $1 - 6\mu$m, and a length is $20\mu$m. In addition to it, a 100 nm Hydrogen contaminant layers placed on the top side of the Al layer. The considered density of the proton is $1n_c$.

The considered size of the simulation box is $60 \times 60\mu\text{m}^2$ ($x \times y$ plan) with simulation mesh size of $dx = 1/50\mu$m and $dy = 1/50\mu$m. Therefore, the box is divided uniformly into $3000 \times 3000$ cells. Furthermore, 240 and 120 particles per cell has taken for Al and H layer, respectively. A circularly-polarized 30 fs (FWHM) laser pulse with a Gaussian profile interact with the target from the left of the box. We have altered the initial position of and propagation angle of the laser pulse to interact with the target in perpendicular (Direction-1) and parallel (Direction-2) direction. The considered laser beam poses a wavelength $\lambda = 0.8\mu$m and a spot $5\mu$m (FWHM), and the normalized amplitude of the laser pulse electric field is $a_0 = 8$ that corresponds to laser intensity $8.8 \times 10^{19}\text{Wcm}^{-2}$. Nevertheless, for further investigation, it extends to $a_0 = 16$ and $a_0 = 24$ that corresponds to $3.5 \times 10^{20}\text{Wcm}^{-2}$ and $8 \times 10^{20}\text{Wcm}^{-2}$, respectively.

## III. RESULTS

The energy spectrum of the accelerated proton beam is shown in Fig.2(a), while a $6\mu$m Al-target irradiated by an ultra-short laser pulse towards the perpendicular to the target as denoted by 'Direction-1' in Fig.1 for various time. The maximum proton energy $\varepsilon_p$ varies from 2.6 MeV to 7.7 MeV for the time being 120 T to 280T. Here, the protons are accelerated due to the plasma sheath field generated at the rear side of the target. The target thickness and density restrict the electrons to acquire sufficient energy to discharge from the target, results in lower $\varepsilon_p$. In this case, the amount of reflected laser energy is higher than absorbed. It should mention here that we have studied the $\varepsilon_p$ spectrum for several target thickness ($1 - 6\mu$m, not shown in the manuscript), yet no significant change in energy observed. On the other hand, similar experimental data have been found in earlier investigations [36–38]. Neely et al. show that the maximum detectable proton energy varies 0.6 MeV to 4 MeV for an aluminum foil thickness of $30\mu$m to $0.1\mu$m for a laser intensity $\sim 10^{19}\text{Wcm}^{-2}$[36]. Whereas, Liao et al. reported that enhanced TNSA proton beams are successfully collected 4-9 MeV proton energy during the interaction of an ultra-intense ($6 \times 10^{19}\text{Wcm}^{-2}$) femtosecond laser pulse with a $2.5\mu$m aluminum target with a contaminated hydrogen layer at the rear surface [37]. Recently, TNSA proton acceleration of 5 MeV to 9 MeV were reported while $6\mu$m Al foil exposed by an ultra-intense ($\sim 10^{20}\text{Wcm}^{-2}$) laser pulse in their experimental

work done by Ter-Avetisyan et al. [38]. A comparative study of our simulation results with the experimental work strongly suggests that the PIC simulation code OPIC 2.0 is able to provide a picture closer to the real experiment investigations.

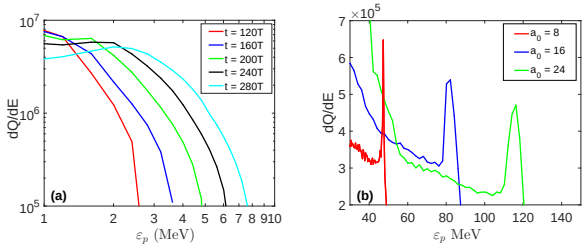


FIG. 2: The energy spectrum of the generated proton beam due to the interaction between plasmas and an ultra-intense laser pulse (a) perpendicular to the Al surface at the (Direction-1) for various time and (b) parallel to the interface of the Al-H junction (Direction-2) at time 120 T for various laser intensities.

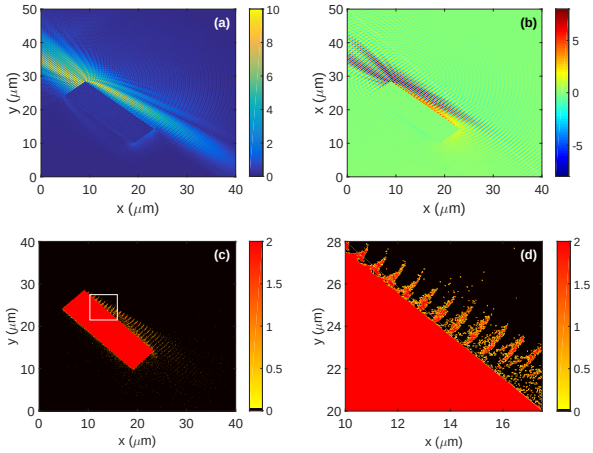


FIG. 3: Spatial distribution of (a) laser amplitude ($a_0 = 8$) while interacting to the target at 70T and (b) corresponding self-generated magnetic field ($B_z$), which causes (c) electron interface structure. (d) A microscopic view of the white-bordered area in (c) helps us to observe the electron Interface wave more clearly.

On the other hand, the scenario changes while the laser beam is incident parallel to the target interface between the Al-foil and the contaminant Hydrogen layer (Direction-2). In this case, a drastic increasing in proton energy is observed, as can be seen in Fig.2(b). The maximum proton energy ($\varepsilon_p$) reaches to 50 MeV (22 times higher) with a sharp cutoff at time 120 T. Moreover, the energy spread is 3 MeV (FWHM) with peak energy at 48 MeV. Consequently, 83MeV and 116MeV peak energy with 5 MeV and 7 MeV energy spreaded proton beams are obtained for laser intensity $3.5 \times 10^{20}\mathrm{Wcm}^{-2}$ (corresponds to $a_0 = 16$) and $8 \times 10^{20}\mathrm{Wcm}^{-2}$ (corresponds to $a_0 = 24$), respectively, at $t = 120T$. The corresponding maximum $\varepsilon_p$ with sharp cutoff is seen at 90 and 120 MeV, respectively, for these cases. On the other hand, the maximum energy of the proton beam can reach only

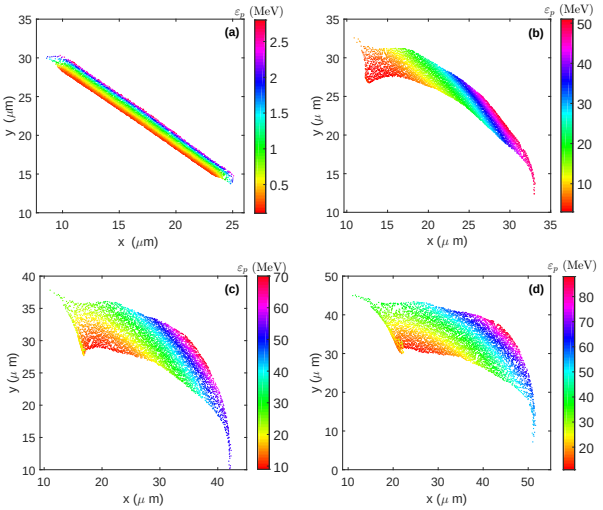


FIG. 4: Energy distribution of the protons due to a laser pulse with intensity $8.8 \times 10^{19}\mathrm{Wcm}^{-2}$ (corresponding to amplitude $a_0 = 8$) from (a) perpendicularly (Direction-1) laser pulse at 120 T; and parallely (Direction-2) laser pulse at (b) 120 T, (c) 160 T, and (d) 200 T.

$\sim$ 4 and $\sim$ 6 MeV, respectively, at the same time for perpendicularly incident (Direction-1) laser pulse.

From the snapshot of the laser amplitude at 70T, shown in Fig.3(a), one can realize that the scattering takes place of reflection for the laser pulse when it hits towards the high density target interface. The intense laser pulse generates a Interface Electron Structure, which leads to the change of the plasma density, so that leads to an increase of absorbance of the laser pulse for the electron acceleration[29]. Electrons gain energy from the longitudinal electric field of the plasma wave and the transverse electric fields of the laser pulse. It causes the self-focusing of the laser beam and results in an stronger electrostatic field. Electrons accelerated by propagating laser pulse towards the channel produce current which generates quasi-static azimuthal magnetic field [39]. The generating magnetic field results in the appearance of electron surface waves (SWs). Spatial distribution of the self-generating magnetic field ($B_z$) illustrated in Fig.3(b). At the same time, the electron surface wave can be observed at the snapshot of the electron density distribution in Fig.3(c). Moreover, it witnessed more clearly in the microscopic view of the small area in Fig.3(c), denoted by a white rectangle, shown in Fig.3(d). We can mark precisely that the electron surface wave poses the same wavelength of the laser pulse. Usually, the properties of the electron surface waves are hugely dependent on the propagation direction [40]. Earlier, the possibility of the existence of magnetoplasma SWs propagated along an external magnetic field (Faraday geometry) in a plasma-metal structure has been indicated and consequently pointed that waves of a surface type existed in a cold electron plasma at frequencies $\omega > \omega_1$ and $\omega < min(\omega_e, \Omega_e)$, where, $\omega_1$ is the upper hybrid frequency, $\omega_e$ is the electron cyclotron frequency, and $\Omega_e$

is the electron plasma frequency [41, 42].

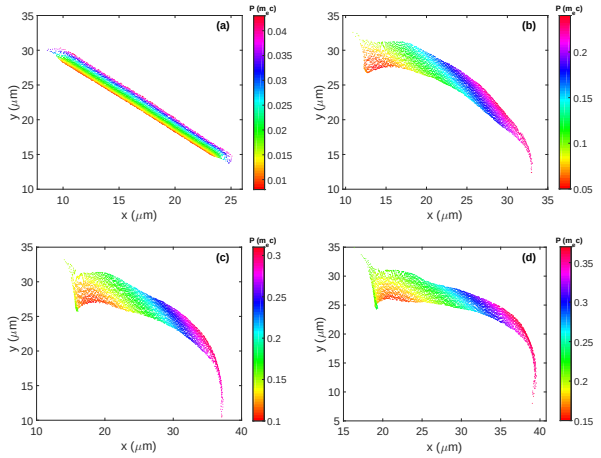


FIG. 5: Relativistic momentum of the accelerated protons at 120T (a) conventional perpendicular incident laser pulse with amplitude $a_0 = 8$ and (b) parallel directed on the surface for the same laser amplitude, wheres, the same diagrams are plotted for (c) $a_0 = 16$ and (d) $a_0 = 24$.

Escaped electrons from the target due to the SW results in a positive charge field around the upper surface of the target. Therefore, a Coulomb's force accelerates the protons to the higher energy. The snapshots of the accelerating protons for parallel (Direction-2) laser pulse at 120T, 160T, and 200T are illustrated in Fig. 4 (b), (c), and (d), respectively, with their respective kinetic energy in MeV. We may perceive that the protons accelerate along normal to the target surface though, the laser interacts towards the parallel to it. Moreover, the accelerated protons gain energy from 50 MeV (at 120 T) to 90 MeV (at 200 T) within a short time, 80T. These aspects refer to that protons are accelerated by Coulomb's force. Fig. 4 (a) also shows the snapshot of TNSA dominant proton distribution in the space-charge field due to the perpendicular (Direction-1) laser pulse at 120T. For further perception, we have plotted the proton distribution in terms of its momentum in Fig.5. Here, Fig.5(a) and (b) reveal the variation of momentum in the space-charge field at 120T when an $8.8 \times 10^{19}\mathrm{Wcm}^{-2}$ intense ($a_0 = 8$) laser pulse interacts perpendicularly (Direction-1) and parallelly (Direction-2) to the target, respectively. The momentum ($P$ in $m_e c$) varies from 0 to $\sim 0.04 m_e c$ for the regular laser incident direction. On the other hand, the protons are accelerated with momentums of $0.05 m_e c$ to $0.24 m_e c$ for our proposed case. These value become higher for the higher intense laser pulses as can be observed in the figure (Fig.5(c) and (d) for $I_0 = 3.5 \times 10^{20}\mathrm{Wcm}^{-2} (a_0 = 16)$ and $I_0 = 8 \times 10^{20}\mathrm{Wcm}^{-2} (a_0 = 24)$, respectively).

On the other hand, the parallel laser beam onward the interface provides another advantage. For a prolonged analysis, it is found that there are no zero or low energetic protons left behind the mainstream. One can observe more clearly from Fig.6, where the time evolution of the energy of the proton beam is plotted. This figure helps us to understand the variation of energy distribution with time. The bar diagram inside the main figure shows the minimum energy ($\varepsilon_p$(min)) of the protons, which increases with time. From the Fig. 4 (a), we may observe that, it is zero at 60T but starts increasing since then, and reaches to 13 MeV at $t = 260T$ whereas the maximum energy ($\varepsilon_p$(max)) varies 8 MeV to 112 MeV for a laser pulse with intensity $8.8 \times 10^{19}\mathrm{Wcm}^{-2}$. Whereas the minimum $\varepsilon_p$ varies from 2 MeV to 102 MeV for a laser pulse with intensity $8 \times 10^{20}\mathrm{Wcm}^{-2}$ in Fig.6(b). The energy spectrum of protons at time $t = 240T$ for different laser intensities is given in Fig.6(c).

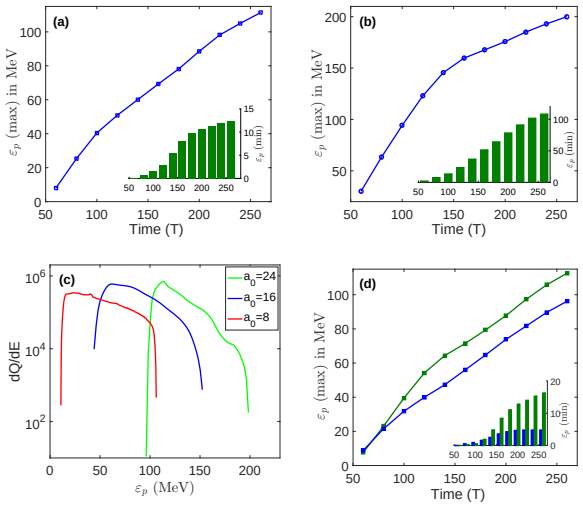


FIG. 6: The evolution of maximum and minimum (inside figure) proton energy ($\varepsilon_p$) with time due to the laser intensity (a) $I_0 = 8.8 \times 10^{19}\mathrm{Wcm}^{-2}$ corresponds to $a_0 = 8$ and (b) $I_0 = 8 \times 10^{20}\mathrm{Wcm}^{-2}$ ($a_0 = 24$). This implies that all the protons are accelerated with time being and no less energetic protons left behind the mainstream (even it can be 102 MeV) as can also be observed from the proton distribution in the space-charge field in Fig.4. (c) Shows the energy spectrums of proton at $t = 240$ T for the interface irradiated parallel by a laser pulse with amplitude $a_0 = 8$, $a_0 = 16$, and $a_0 = 24$ respectively. (d) is for the angle variation in either direction from the exact parallel direction. Here, The green (blue) line indicates the 5° variation towards the surface front (back) direction.

Furthermore, we have also made some investigations for varying the incident angle of the laser pulse ($I_0 = 8.8 \times 10^{19}\mathrm{Wcm}^{-2}$) around ±5° from the parallel direction. It is found that the 5° shift along the target surface results in higher minimum $\varepsilon_p$, though the maximum $\varepsilon_p$ remains the same. However, the 5° along the interface back, i.e., −5° results in lower average kinetic energy with $\varepsilon_p$(max) and $\varepsilon_p$(min), because of more reflection of laser pulse. It should be noticed that −90° corresponding to 'Direction-1' case.

## IV. CONCLUSION

We have investigated the proton acceleration due to the parallel incident laser pulse towards the interface between high density plasma and low density plasma. For this purpose, we adopted the density of the aluminum target with 2.7 gm/cc and 100 nm thick contaminant Hydrogen layer is chosen as a source of the protons. First of all, we made a comparative study of our data yield from our PIC simulation for a laser pulse incident towards perpendicular (Direction-1) to the target at the opposite surface of the contaminant Hydrogen layer, to experimental data. The similarity of results from the above two sources fortifies us to go ahead further.

A laser beam propagating parallel to the adjoining interface produces an Interface Plasma Wave. Consequently, the frequency of the IPWs identical to the incident laser pulse. The IPW pulled out a large number of electrons from the target results in a positively charged field. Therefore, protons are accelerated by the means of Coulomb's repulsive force to $\sim 20$ times higher or even more depending on the laser intensity. An ultra-intense laser pulse irradiating parallel to the plasmas interface to produce a larger amplitude surface plasma wave which enhance markedly sheath electric field to accelerate efficiently proton, and reduce reflection of laser pulse to improve the couple efficiency. As results, the proton beam has three advantages: (1) with higher peak energy, (2) A sharp peak with $\sim 3$ MeV energy spread and razor-sharp cutoff, (3) no lower or zero energetic protons left behind the mainstream, because of longer time acceleration.

Moreover, it shows the flexibility of incident angle of the laser pulse on the target. $5^\circ$ angle variation in both sides also shows its efficiency in the almost same manner with tiny changes in maximum and minimum proton energy.

This is a high efficient, robust and easier realized scheme to produce high quality proton beam, which is desirable in applications such as laser-driven fast ignition, cancer treatment, and proton photography etc.

### Acknowledgments

We would like to thank Dr. D Wu for his helpful discussion. This work was supported by the National Natural Science Foundation of China (NNSFC) under Grant Nos. 11475147, 61627901, and 11875235.

[1] A. P. Fews, P. A. Norreys, F. N. Beg, A. R. Bell, A. E. Dangor, C. N. Danson, P. Lee, and S. J. Rose, *Phys. Rev. Lett.* **73**, 1801 (1994).
[2] E. L. Clark, K. Krushelnick, J. R. Davies M. Zepf, M. Tatarakis, F. N. Beg, A. Machacek, P. A. Norreys, M. I. K. Santala, I. Watts, and A. E. Dangor, *Phys. Rev. Lett.* **84**, 670 (2000).
[3] A. Maksimchuk, K. Flippo, H. Krause, G. Mourou, K. Nemoto, D. Shultz, D. Umstadter, R. Vane, V. Yu. Bychenkov, G. I. Dudnikova, V. F. Kovalev, K. Mima, V. N. Novikov, Y. Sentoku, and S. V. Tolokonnikov, *Plasma Phys. Rep.* **30**, 473 (2004).
[4] M. S. Wei, J. R. Davies, E. L. Clark, F. N. Beg, A. Gopal, M. Tatarakis, L. Willingale, P. Nilson, A. E. Dangor, P. A. Norreys, M. Zepf, and K. Krushelnick, *Phys. Plasmas* **13**, 123101 (2006).
[5] T. Esirkepov, M. Borghesi, S. V. Bulanov, G. Mourou, and T. Tajima, *Phys. Rev. Lett.* **92**, 175003 (2004).
[6] A. P. L. Robinson, M. Zepf, S. Kar, R. G. Evans, and C. Bellei, *New J. Phys.* **10**, 013021 (2008).
[7] Y. I. Salamin, *Phys. Rev. A* **92**, 063818 (2015).
[8] Y. Xu, J. Wang, H. Hora, X. Qi, Y. Xing, L. Yang, and W. Zhu, *Phys. Plasmas* **25**, 043102 (2018).
[9] J. Ferri, L. Senje, M. Dalui , K. Svensson, B. Aurand, M. Hansson , A. Persson, O. Lundh , C.-G. Wahlstrm, L. Gremillet , E. Siminos, T. C. DuBois , L. Yi, J. L. Martins, and T. Flp, *Phys. Plasmas* **25** 043115 (2018).
[10] Marco Borghesi,'Ion Acceleration: TNSA and Beyond' in L. A. Gizzi, R. Assmann, P. Koester, and A. Giulietti (Ed.), Laser-Driven Sources of High Energy Particles and Radiation,*Springer International Publishing* (2019).
[11] M. Afshari, J. Hornung, A. Kleinschmidt, P. Neumayer, D. Bertini, and V. Bagnoud *AIP Advances* **10**, 035023 (2020).
[12] A. Macchi, M. Borghesi, and M. Passoni, *Rev. Mod. Phys.* **85**, 751 (2013).
[13] M. Cerchez, M. Swantusch, M. Toncian, X. Zhu, R. Prasad, T. Toncian, C. Rodel, O. Jackel, G. G. Paulus, A. Andreev, and O. Willi, *Appl. Phys. Lett.* **112**, 221103 (2018).
[14] X. M. Zhu, R. Prasad, M. Swantusch, B. Aurand, A. A. Andreev, O. Willi, and M. Cerchez, *High Power Laser Science and Engineering* **8**, 15, 10 (2020).
[15] A. L. Giesecke, C. Peth, T. Toncian, O.Willi, and M. Cerchez, *Laser Part. Beams* **37**, 12 (2019).
[16] A. Macchi, *Phys. Plasmas* **25**, 031906 (2018).
[17] S. R. Seshardi, *IRE Trans., MTT-10* **6**, 573(1962).
[18] M. Toda, *J. Phys. Soc. Jpn.* **19**, 7, 1126 (1964).
[19] R. Hirota, *J. Phys. Soc. Jpn.* **19**, 7, 1130 (1964).
[20] R. Hirota and K. Suzuki, *J. Phys. Soc. Jpn.* **21**, 6, 1112 (1966).
[21] N. A. Azarenkov, A. N. Kondratenko, and K. N. Ostrikov, *Radiophysics and Quantum Electronics* **36**, 5 (1993).
[22] P. Chauhan, D. A. Varshney and V. Sajal, *Laser Part. Beams* **33** 109 (2015).
[23] Mehdi Abedi-Varaki, *Mod. Phys. Lett. B* **33**, 23, 1950267(2019).
[24] D. J. Cooperberg, *Phys. Plasmas* **5**, 853 (1998).
[25] A. Sgattoni, L. Fedeli, G. Cantono, T. Ceccotti, and A. Macchi, *Plasma Phys. Control. Fusion* **58**, 014004 (2016).
[26] M. Raynaud, J. Kupersztych, C. Riconda, J. Adam, and A. Heron, *Phys. Plasmas* **14**, 092702 (2007).
[27] L. Fedeli, A. Formenti, L. Cialfi, A. Sgattoni, G. Cantono, and M. Passoni, *Plasma Phys. Control. Fusion* **60**,

014013 (2018).
[28] G. Cantono, A. Sgattoni, L. Fedeli, D. Garzella, F. Reau, C. Riconda, A. Macchi, and T. Ceccotti, *Phys. Plasmas* **17**,093105 (2018).
[29] C. Liu, V. Tripathi, X. Shao, and T. Liu, *Phys. Plasmas* **22** 023105 (2015).
[30] Z. M. Zhang, X. T. He, Z. M. Sheng, and M. Y. Yu, *Phys. Plasmas* **17**, 043110 (2010).
[31] Z. M. Zhang, X. T. He, Z. M. Sheng, and M. Y. Yu, *P*hys. Plasmas **1**8, 023110 (2011).
[32] Z. M. Zhang, X. T. He, Z. M. Sheng, and M. Y. Yu, *Appl. Phys. Lett.* **100**, 134103 (2012).
[33] S. F. Tong, Z. M. Sheng, and M. Y. Yu, *Phys. Rev. Accel. Beams* **21**, 051303 (2018).
[34] S. F. Tong, Z. M. Sheng, and M. Y. Yu, with thin double-layer target *Phys. Plasmas* **26**, 033103 (2019).
[35] O. Rahman,S. F. Tong, and Z. M. Sheng, *Phys. Plasmas* **27**, 033107, (2020).
[36] D. Neely, P. Foster, A. Robinson, F. Lindau, O. Lundh, A. Persson, C.-G. Wahlstrm, and P. McKenna, *Appl. Phys. Lett.* **89**, 021502 (2006).
[37] Q. Liao, M. J. Wu, Z. Gong, Y. X. Geng, X. H. Xu, D. Y. Li, Y. R. Shou, J. G. Zhu, C. C. Li, M. Yang, T. S. Li, H. Y. Lu, W. J. Ma, Y. Y. Zhao, C. Lin, and X. Q. Yan, *Phys. Plasmas* **25**, 063109 (2018).
[38] S. Ter-Avetisyan , P. K. Singh , M. H. Cho, A. Andreev, K. F. Kakolee, H. Ahmed, C. Scullion , S. Sharif, P. Hadjisolomou, and M. Borghesi, *Phys. Plasmas* **26**, 103106 (2019).
[39] I. Tsymbalov, D. Gorlova, S. Shulyapov, V. Prokudin, A. Zavorotny,K. Ivanov, R. Volkov, V. Bychenkov, V. Nedorezov, A. Paskhalov,N. Eremin and A. Savelev, *Plasma Phys. Control. Fusion* **61** 075016 (2019).
[40] N. A. Azarenkov, A. N. Kondratenko, and K. N. Ostrikov *Radiophysics and Quantum Electronics* **36**, 5, (1993).
[41] A. B. Davydov and V. A. Zakharov, *Fiz. Tverd. Tela,* **17**, 1, 201 (1975).
[42] P. Halevi, *Phys. Rev. B* **23**, 6, 2635 (1981).